Hybrid adaptive filter for full optical current transformer system based on tristate polarization diversity receiver

QING TAO[a,b], BOWEN LU[a], CHEN HU[a], XIN YU[a], ZHONGSHENG ZHAI[a,b], JIAN CHENG[a], DUN LIU[a,*]
[a]*School of Mechanical Engineering, Hubei University of Technology, Wuhan 430068, China*
[b]*Hubei Key Laboratory of Modern Manufacturing Quantity Engineering, School of Mechanical Engineering, Hubei University of Technology, Wuhan 430068, Hubei, P.R. China*

In this paper, a new hybrid adaptive filter for all fiber current transformer system based on tristate polarization diversity receiver is researched. The entire system is a fully polarized system. Based on the optical pulse interference modulation and demodulation, the tristate polarization diversity receiver and hybrid adaptive filter are used to reduce the current ratio errors. It can be seen that in the 60A@50Hz current grade, ratio errors obtained by new method is less nearly 3 times than by traditional scheme. In the 240A@50Hz current grade, ratio errors obtained by new method is less almost 1.4 times than by traditional scheme. In the 1200A@50Hz current grade, ratio errors obtained by new method is less nearly 1.3 times than by traditional scheme. The new method can be best applied to high current sensing system and improve its stability.

(Received July 31, 2019; accepted February 17, 2020)

Keywords: Polarization diversity receiver, Full optical current transformer, Phase generation carrier, Adaptive variable step size recursive least square method, CL multi-wavelet

1. Introduction

In this paper, the proposed new system is different from the traditional full optical current transformer system (FOCTS) [1-4]. The traditional current sensor system is based on continuous optical interference scheme, but the new system is based on polarized optical pulse interference scheme.

And, the hybrid adaptive filter is used into the new system, which is based on CL multi-wavelet [5] composed with adaptive variable step size recursive least square (RLS) [6-7] method for the FOCTS [8-9]. Although some filters in the current transformer system [10-13] are studied, few article focus on the hybrid adaptive filter based on tristate polarization diversity receiver for the FOCTS. The new FOCTS reduces the optical and electrical noise in the whole system. So, the fluctuation of ratio errors is compressed to between 1/3 and 1/1.3 times for different current size grades. Testing results have good stability between -40°C and 75°C in the new system. The new method can be best applied to high current sensing system.

2. Theoretical model of hybrid adaptive filter for the FOCTS

Because the reflective FOCTS is relatively insensitive to temperature variation, fiber vibration and distortion [14], we propose a new full optical current transformer structure in the Fig. 1 to meet the 0.2s national standard.

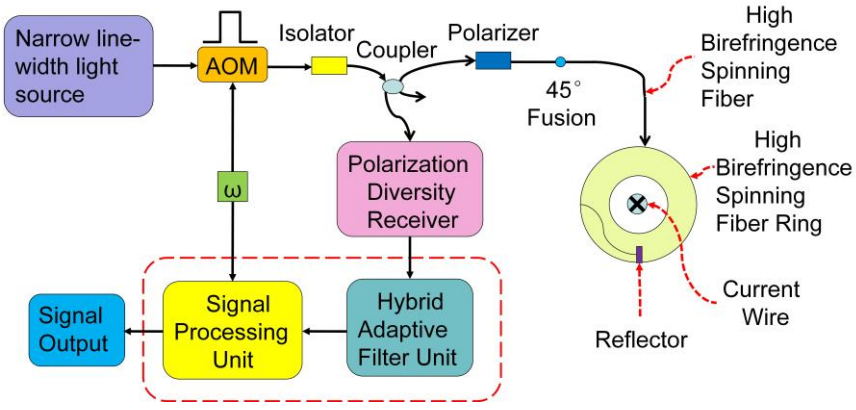

Fig. 1. All fiber current transformer structure (color online)

In Fig. 1, the center wavelength of light pulse is 1490 nm. light emitted from narrow-line-width light source is modulated by acousto-optic modulator to form an optical pulse and instantaneous power of optical pulse is 50 mW. Firstly, optical pulse is transmitted to isolator to cut off the reflected light. Then, the optical pulse is transmitted to polarization maintaining (PM) fiber coupler to form an upward and downward light paths. Secondly, the descending optical pulse is linearly polarized by polarizer. Then, optical pulse is transmitted to the X-axis and Y-axis of PM fiber through 45° fusion. Two orthogonal linearly polarized lights form left-rotated and right-rotated circularly polarized light when optical pulse has passed through a high birefringence spinning fiber. During two circularly polarized lights transmitting in the high birefringence spinning fiber, Faraday magneto-optical effect produces a phase difference Φ between left-rotated and right-rotated circularly polarized light. The reflective mirror draws back two circularly polarized lights to the original high birefringence spinning fiber, the phase difference Φ is doubled. Two circular polarization lights become two linearly polarized lights propagating along X-axis and Y-axis, then, optical interferring signal is formed through the 45° fusion point. The polarized light passes through the polarizer and PM fiber coupler again to enter the polarization diversity receiver (PDR) [15-18]. The signal eliminated the polarization fading enters the adaptive hybrid filter and signal processing units. Afterwards, an inverse tangent-based phase generation carrier (PGC) [19] demodulation calculation is performed, and the measured current magnitude is obtained in the Fig. 2.

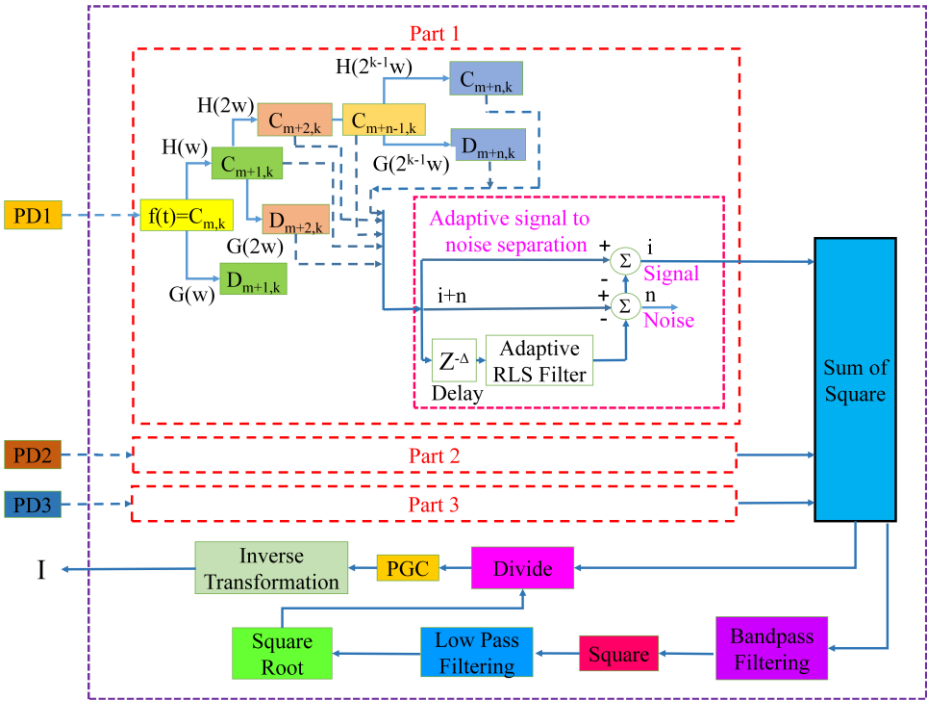

Fig. 2. Hybrid adaptive filter and signal processing unit (color online)

When optical pulse signal with phase difference enters the tristate PDR, each signal enters hybrid adaptive filter, respectively, which is part1, part2 and part3 in the Fig. 2. Optical signal is decomposed to third order structure by CL multi-wavelet [20-21] transformation. The maximum minimum threshold method [22-23] is used to rebuild high frequency wavelet coefficients for each order. The low frequency wavelet coefficients are filtered by adaptive variable step-size RLS filter for each order [24-25]. New optical signal is obtained by CL multi-wavelet inverse transformation. Then, three new optical signals are squared and summed. After bandpass filtering, total power is squared again. Then low-pass filtering, new squared result is divided with above summation. The result is inputted into the arctangent PGC unit, phase difference is calculated. The measured current is obtained by inverse Faraday magneto-optical effect.

Assumed that two interfering light pulses $\vec{E}_s$ and $\vec{E}_r$ are linearly polarized, elliptic angles $\varepsilon_s=0$ and $\varepsilon_r=0$. E_s, E_r and ϕ_s, ϕ_r are amplitudes and phases of $\vec{E}_s$ and $\vec{E}_r$. θ_s and θ_r are azimuth angles. Subscript s, r indicate two interfering lights, respectively. E_{sx} and E_{rx} are components of E_s and E_r in x axis. E_{sy} and E_{ry} are components of E_s and E_r in y axis.

The Jones matrix expression is,

$$\begin{bmatrix} E_{sx} \\ E_{sy} \end{bmatrix} = E_s \exp\left(j\phi_s\right) \begin{bmatrix} \cos\theta_s \\ \sin\theta_s \end{bmatrix} \tag{1}$$

$$\begin{bmatrix} E_{rx} \\ E_{ry} \end{bmatrix} = E_r \exp\left(j\phi_r\right) \begin{bmatrix} \cos\theta_r \\ \sin\theta_r \end{bmatrix} \tag{2}$$

When the linearly polarized optical signal with interfering information passes through the photodetector, the linearly polarized optical pulse forms θ angle with photodetector. Then, matrix of θ angle is,

$$\vec{E}_d = \begin{pmatrix} \cos\theta \\ \sin\theta \end{pmatrix} \tag{3}$$

Instantaneous light intensity I is,

$$I = \left|\vec{E}_s \cdot \vec{E}_d + \vec{E}_r \cdot \vec{E}_d\right|^2 \tag{4}$$

Because I is power sequence with time, I can be expressed as discrete noise-containing signal sequence $A(n)$.

Firstly, $A(n)$ is vectorized,

$$A(n) = \begin{bmatrix} a_{2n-1} \\ a_{2n} \end{bmatrix}, \ n = 1, 2, \cdots, \frac{N}{2} \tag{5}$$

Then, $A(n)$ is prefiltered,

$$B(n) = \sum_k P_{re}(k) A(n-k) = \begin{bmatrix} b_n \\ b_{\frac{N}{2}+n} \end{bmatrix} \tag{6}$$

$$n = 1, 2, \cdots, \frac{N}{2}$$

Here,

$$P_{re}(k) = \begin{bmatrix} 1/4 & 1/4 \\ \dfrac{1}{1+\sqrt{7}} & \dfrac{-1}{1+\sqrt{7}} \end{bmatrix} \tag{7}$$

CL multi-wavelet transform is implemented on low frequency part of $B(n)$, marked as $B^L(n)$.

$$B^L(m) = \sum_n H(n-2m) B(n) = \begin{bmatrix} b_m^L \\ b_{\frac{N}{4}+m}^L \end{bmatrix} \tag{8}$$

$$m = 1, 2, \cdots, \frac{N}{4}$$

$H(n)$ is low-pass parameters,

$$H(0) = \begin{bmatrix} 1/2\sqrt{2} & -1/2\sqrt{2} \\ -1/4\sqrt{2} & 1/4\sqrt{2} \end{bmatrix}$$

$$H(1) = \begin{bmatrix} -1/\sqrt{2} & 0 \\ 0 & \sqrt{7}/2\sqrt{2} \end{bmatrix}$$

$$H(2) = \begin{bmatrix} 1/\sqrt{2} & 1\sqrt{2} \\ 1/4\sqrt{2} & 1/4\sqrt{2} \end{bmatrix}$$

CL multi-wavelet transform is implemented on high frequency part of $B(n)$, marked as $B^H(n)$.

$$B^H(m) = \sum_n G(n-2m) B(n) = \begin{bmatrix} b_m^H \\ b_{\frac{N}{4}+m}^H \end{bmatrix} \tag{9}$$

$$m = 1, 2, \cdots, \frac{N}{4}$$

$G(n)$ is high-pass parameters,

$$G(0) = \begin{bmatrix} 1/\sqrt{2} & -1/\sqrt{2} \\ \sqrt{7}/4\sqrt{2} & -\sqrt{7}/4\sqrt{2} \end{bmatrix}$$

$$G(1) = \begin{bmatrix} -1/\sqrt{2} & 0 \\ 0 & \sqrt{7}/2\sqrt{2} \end{bmatrix}$$

$$G(2) = \begin{bmatrix} 1/2\sqrt{2} & -1/2\sqrt{2} \\ -\sqrt{7}/2\sqrt{2} & -\sqrt{7}/2\sqrt{2} \end{bmatrix}$$

CL multi-wavelet decomposition of noise-containing signal is obtained.

$$\begin{gathered} A(n) = \left[a_1 a_2 \cdots a_N\right] \Rightarrow \\ \left[b_1^L \cdots b_{\frac{N}{2}}^L \ b_1^H \cdots b_{\frac{N}{2}}^H\right] = \left[L \ \ H\right] \end{gathered} \tag{10}$$

Similarly, $D(n)$ is a reference signal sequence.

$$\begin{gathered} D(n) = \left[d_1 d_2 \cdots d_N\right] \Rightarrow \\ \left[e_1^L \cdots e_{\frac{N}{2}}^L \ e_1^H \cdots e_{\frac{N}{2}}^H\right] = \left[L \ \ H\right] \end{gathered} \tag{11}$$

Then, b_i^H and e_i^H are calculated according to threshold value w. The w depends on discrete sample value N,

$$w = \begin{cases} 0, & N \le 32 \\ 0.3936 + \dfrac{0.1829 \ln N}{\ln 2}, & N > 32 \end{cases} \tag{12}$$

Here, $N = 64$. Low frequency part of signal, b_i^L and e_i^L, are filtered by an adaptive variable

step-size RLS filter.

$y(n)$ is low frequency part of signal sequence, $x(n)$ is expected value sequence, $e_1(n)$ is prior estimate error sequence,

$$y(n)=b_i^L=\left[b_1^L\cdots b_{\frac{N}{2}}^L\right] \tag{13}$$

$$x(n)=e_i^L=\left[e_1^L\cdots e_{\frac{N}{2}}^L\right] \tag{14}$$

$R(n)$ is correlation matrix sequence of input vector, $\omega(n)$ is weighted coefficient sequence. $d_i(n)$ is actual output sequence of equalizer, k(n) is Kalman gain vector sequence. $\lambda(n)$ is forgetting factor sequence, $NINT$ means taking integer closest to $p\xi^2(n)$. Adaptive variable step size RLS filter is modified by following equations.

$$d_i(n)=w^T(n-1)y(n) \tag{15}$$

$$\xi(n)=x(n)-d_i(n) \tag{16}$$

$$k(n)=\frac{R^{-1}(n-1)y(n)}{\lambda+y^T(n)R^{-1}(n-1)y(n)} \tag{17}$$

$$R^{-1}=\frac{1}{\lambda}\left[R^{-1}(n-1)-k(n)y^T(n)R^{-1}(n-1)\right] \tag{18}$$

$$w(n)=w(n-1)+k(n)\overset{*}{\xi}(n) \tag{19}$$

$$\lambda(n)=\lambda_{\min}+(1-\lambda_{\min})a^{L(n)} \tag{20}$$

$$L(n)=-NINT\left[p\xi^2(n)\right] \tag{21}$$

Here, $a=0.75$, $p=0.75$ and $\lambda_{\min}=\lambda(n)/6$.

Similarly, high frequency part of signal, b_i^H and e_i^H ,are also filtered by an adaptive variable step-size RLS filter.

Assumed that, $y_1(n)=d_1(n)$ and $y_2(n)=d_2(n)$. CL multi-wavelet coefficients are reconstructed by following equation,

$$g_k=\sqrt{2}\sum_{n\in Z}\overset{*}{H}_{k-2n}y_1(n)+\overset{*}{G}_{k-2n}y_2(n) \tag{22}$$

$y_3(n)$ is obtained and g_k is its elements.

Then, $y_3(n)$ is post-filtered,

$$G(n)=\sum_k P_{af}(k)y_3(n-k)=\begin{bmatrix}g_n\\ g_{\frac{N}{2}+n}\end{bmatrix}\quad n=1,2,\cdots,\frac{N}{2} \tag{23}$$

The sequence of elements is reorganized in the $G(n)$.

Then,

$$G'(n)=\left[g_1,g_{\frac{n}{2}};g_2,g_{\frac{n}{2}+1};\cdots\right] \tag{24}$$

$G'(n)$ contains interference items I',

$$\begin{aligned}I'=&\left(E_{rx}E_{sx}^*+E_{sx}E_{rx}^*\right)\cos^2\theta+\\&\left(E_{sy}E_{ry}^*+E_{sy}^*E_{ry}\right)\sin^2\theta+\\&(E_{ry}E_{sx}^*+E_{ry}^*E_{sx}\\&+E_{rx}E_{sy}^*+E_{rx}^*E_{sy})\sin\theta\cos\theta\end{aligned} \tag{25}$$

Here, $\phi=\phi_s-\phi_r$ is phase difference between two interferometers.

Then,

$$I'=E_sE_r\left(a\cos\phi+b\ \sin\phi\right) \tag{26}$$

$$\begin{aligned}a&=\cos\left(\theta_s-\theta_r\right)+\cos\left(\theta_s+\theta_r-2\theta\right)\\b&=\sin\left(\theta_s-\theta_r\right)+\sin\left(\theta_s+\theta_r-2\theta\right)\end{aligned} \tag{27}$$

Optical power in tristate PDR is I_k,

$$\begin{aligned}I_k=&\frac{1}{n}E_sE_r[\cos\left(\theta_s-\theta_r\right)\\&+\cos\left(\theta_s+\theta_r-2\theta\right)]\cos\phi\end{aligned} \tag{28}$$

Here, $\theta=\dfrac{\pi k}{n}$, $n=3,k=0,....2.$

I_{T} is sum of square,

$$\begin{aligned}I_{\mathrm{T}}&=\sum_{k=0}^{n-1}I_k^2\\&=\frac{2}{n^2}E_s^2E_r^2\left(\cos2\phi+1\right)\times\\&\sum_{k=0}^{n-1}\left[\cos\left(\theta_s-\frac{\pi k}{n}\right)\cos\left(\theta_r-\frac{\pi k}{n}\right)\right]^2\end{aligned} \tag{29}$$

Assumed that,

$$\begin{aligned}&\Phi\left(E_s,E_r,\theta_s,\theta_r\right)=\\&\frac{2}{n^2}E_s^2E_r^2\times\\&\sum_{k=0}^{n-1}\left[\cos\left(\theta_s-\frac{\pi k}{n}\right)\cos\left(\theta_r-\frac{\pi k}{n}\right)\right]^2\end{aligned} \tag{30}$$

Then,

$$\begin{aligned}I_{\mathrm{T}}=&\Phi\left(E_s,E_r,\theta_s,\theta_r\right)+\\&\Phi\left(E_s,E_r,\theta_s,\theta_r\right)\cos\left(2\phi(t)\right)\end{aligned} \tag{31}$$

Another,

$$\begin{aligned}\varphi(t)&=C'\cos\omega_0t+\Omega(t)\\\Omega(t)&=D\cos\omega_st+\varphi_0(t)\end{aligned} \tag{32}$$

Here, $C'=1.315$. ω_0 is the carrier frequency of signal, ω_s is the frequency of sensing signal and $\varphi_0(t)$ is phase difference caused by external environment.

Then,

$$I_T \approx I_T' = \Phi(E_s, E_r, \theta_s, \theta_r) \{1+\cos[C\cos\omega_0 t + 2\Omega(t)]\} \tag{33}$$

$C=2C'=2.63$, and, modulation requirements is,

$$J_1(C)=J_2(C) \tag{34}$$

Expanding formula (34) with Bessel function,

$$\begin{aligned} I_T' = {} & \Phi(E_s, E_r, \theta_s, \theta_r)\times \\ & \{1+J_0(c)\cos(2\Omega(t))+ \\ & \sum_{k=1}^{\infty}(-1)^k J_{2k}(C)\times[\cos(2k\omega_0 t+2\Omega(t)) \\ & +\cos(2k\omega_0 t-2\Omega(t))]- \\ & \sum_{k=0}^{\infty}(-1)^k J_{2k+1}(C)[\sin((2k+1)\omega_0 t \\ & +2\Omega(t))-\sin((2k+1)\omega_0 t-2\Omega(t))] \end{aligned} \tag{35}$$

Here, $\Delta f=\frac{1}{2}f_0=4kHz$, bandwidth of bandpass filter is $(f_0-\Delta f, 2f_0+\Delta f)$.

Above formula goes through bandpass filter,

$$\begin{aligned} I_{T1}' = {} & -2\Phi(E_s, E_r, \theta_s, \theta_r)\times \\ & [J_2(C)\cos(2\omega_0 t)\cos(2\Omega(t))+ \\ & J_1(C)\cos(\omega_0 t)\sin(2\Omega(t))] \end{aligned} \tag{36}$$

Then, I_{T1}' passes through the low-pass filter,

$$\begin{aligned} I_{T2}' = {} & 4\Phi(E_s, E_r, \theta_s, \theta_r)^2 \\ & [J_2^2(C)\cos^2(2\Omega(t))+ \\ & J_1^2(C)\sin^2(2\Omega(t))] \end{aligned} \tag{37}$$

Let be,

$$J_1(C)=J_2(C) \tag{38}$$

And,

$$\cos^2(2\Omega(t))+\sin^2(2\Omega(t))=1 \tag{39}$$

Then,

$$I_{T2}' = 2\Phi^2(E_s, E_r, \theta_s, \theta_r)[J_1^2(C)] \tag{40}$$

Afterwards, formula (40) is squared root,

$$I_{T3}' = \sqrt{2}\Phi(E_s, E_r, \theta_s, \theta_r)[J_1(C)] \tag{41}$$

Dividing I' by I_{T3}'.

$$I_4' = \frac{\sqrt{2}}{2J_1(C)}\{1+\cos[C\cos\omega_0 t+2\Omega(t))]\} \tag{42}$$

Then, I_4' goes through an arctangent PGC system,

$$\begin{aligned} I_4' = {} & \frac{\sqrt{2}}{2J_1(C)}+\frac{\sqrt{2}}{2J_1(C)}\times \\ & \{\left[J_0(C)+2\sum_{k=1}^{\infty}(-1)^k J_{2k}(C)\cos(2k\omega_0 t)\right]\times \\ & \cos(2\Omega(t))-2\times \\ & \left[\sum_{k=0}^{\infty}(-1)^k J_{2k+1}(C)\cos(2k+1)\omega_0 t\right]\times \\ & \sin(2\Omega(t))\} \end{aligned} \tag{43}$$

Here, $k=0,1$,

So,

$$\begin{aligned} I_4' = {} & \frac{\sqrt{2}}{2J_1(C)}+\frac{\sqrt{2}}{2J_1(C)} \\ & \{J_0(C)\cos(2\Omega(t))- \\ & 2J_2(C)\cos(2\omega_0 t)\cos(2\Omega(t)) \\ & -2J_1(C)\cos(\omega_0 t)\sin(2\Omega(t))\} \end{aligned} \tag{44}$$

Multiplying $\cos\omega_0 t$ on both sides of formula (44).

$$\begin{aligned} I_5' = {} & \frac{\sqrt{2}}{2J_1(C)}\cos(\omega_0 t)+\frac{\sqrt{2}}{2J_1(C)}\times \\ & [\{J_0(C)\left(\frac{\cos(2\Omega(t)+\omega_0 t)+\cos(2\Omega(t)-\omega_0 t)}{2}\right) \\ & -J_2(C)((\frac{\cos(2\Omega(t)+3\omega_0 t)+\cos(3\omega_0 t-2\Omega(t))}{2} \\ & +\frac{\cos(2\Omega(t)+\omega_0 t)+\cos(2\Omega(t)-\omega_0 t)}{2}))- \\ & 2J_1(C)((\frac{\sin(2\Omega(t)+2\omega_0 t)-\sin(2\omega_0 t-2\Omega(t))}{2}) \\ & +\sin(2\Omega(t)))\}] \end{aligned}$$

After low-pass filtering, $2f_s$ is frequency of $2\Omega(t)$, and $2f_s \ll f_0$.

Above equation is simplified to I_6'.

$$I_6' = -\sqrt{2}\sin(2\Omega(t)) \tag{45}$$

Similarly, multiplying $\cos(2\omega_0 t)$ on both sides of formula (44).

$$I_7' = \frac{\sqrt{2}}{2J_1(C)}\cos(2\omega_0 t) + \frac{\sqrt{2}}{2J_1(C)} \times \left[\left\{J_0(C)\left(\frac{\cos(2\Omega(t)+2\omega_0 t)+\cos(2\Omega(t)-2\omega_0 t)}{2}\right)\right.\right. - J_2(C)\left(\frac{\cos(2\Omega(t)+4\omega_0 t)+\cos(2\Omega(t)-4\omega_0 t)}{2} - J_2(C)\cos(2\Omega(t))\right) - J_1(C)\left(\left(\frac{\sin(3\omega_0 t+2\Omega(t))-\sin(3\omega_0 t-2\Omega(t))}{2}\right)\right. \left.\left.\left. + \left(\frac{\sin(2\omega_0 t+2\Omega(t))-\sin(2\omega_0 t-2\Omega(t))}{2}\right)\right)\right\}\right] \quad (46)$$

I_7' passes through a low-pass filter, equation is simplified to I_8'.

$$I_8' = -\frac{\sqrt{2}}{2}\cos(2\Omega(t)) \quad (47)$$

Dividing I_8' with I_6'.

$$I_9' = 2\tan(2\Omega(t)) \quad (48)$$

Simplifying formula (48),

$$\Omega(t) = \frac{acr\tan(I_9'/2)}{2} \quad (49)$$

Formula (49) is introduced into current and phase relational equation,

$$\Omega(t) = 4NVI(t) \quad (50)$$

Then, current amplitude with time, $I(t)$ can be calculated.

$$I(t) = \frac{\Omega(t)}{4NV} \quad (51)$$

3. Experimental results and discussion

The new FOCTS is placed in the temperature control box for high and low temperature test. The testing method [26] is as shown in the Fig. 3.

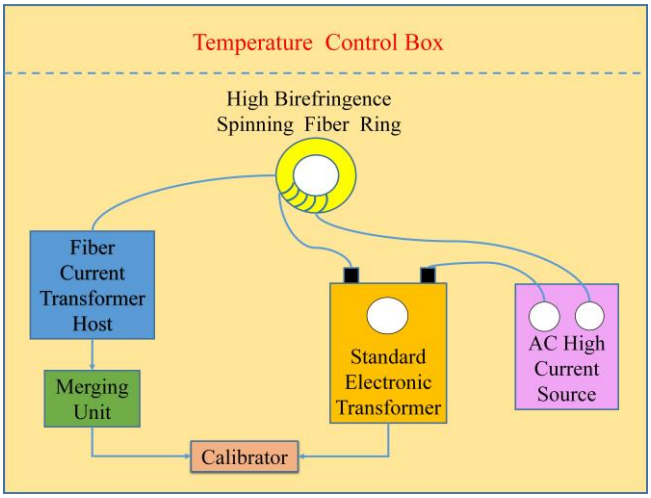

Fig. 3. Performance testing structure for full optical current transformer system (color online)

This system includes merging unit, high birefringence spinning fiber ring, fiber current transformer host, standard electronic transformer, alternating current (AC) high current source and calibrator. The formula of current ratio error is

$$\beta = \frac{(I_b M - I_a)\times 100}{I_a} \quad (52)$$

β is current ratio error, I_a and I_b are real primary current and real secondary current, respectively, and M is rated current ratio. High birefringence spinning fiber ring whose main function is to collect current signal. The function of fiber current transformer host is signal modulation and calculation, acquired result outputs to merging unit. Calibrator compares the measured electric current with standard electric current obtained by electronic transformer. Merging unit obtains the ratio error under the conditions that temperature periodically and quickly changes between -40°C and 75°C for almost ten minutes.

In Fig. 4, red symbol '-+-' curve indicates temperature change. Blue symbol '---' curve shows ratio error variation at the earlier FOCTS [27]. Pink symbol '-*-' curve displays improved ratio error, where Haar wavelet combined with RLS filter is used. Black symbol '-.-' curve indicates improved ratio error, in which CL multi-wavelet combined with adaptive variable step-size RLS filter is used.

In Fig. 4 (a), it can be seen that current size is 60A, fluctuation of ratio error marked by blue symbol '---' curve is within ±0.6%. Fluctuation of ratio error marked by pink symbol '-*-' curve is within ±0.25%. Fluctuation of ratio error marked by black symbol '-.-' curve is within ±0.2%. It can be seen that three experimental results meet national standards, where fluctuation of ratio error is within ± 0.75%. However, the result based on CL multi-wavelet combined with variable step-size RLS filter is best, where fluctuation value of ratio error is within ±0.2%. The result

based on Haar wavelet combined with conventional RLS filter is better, where fluctuation value of ratio error is relatively more ±0.5% than those obtained by the first method. The result based on traditional system is the last, where fluctuation value of ratio error is relatively more ±0.35% than those obtained by the second method.

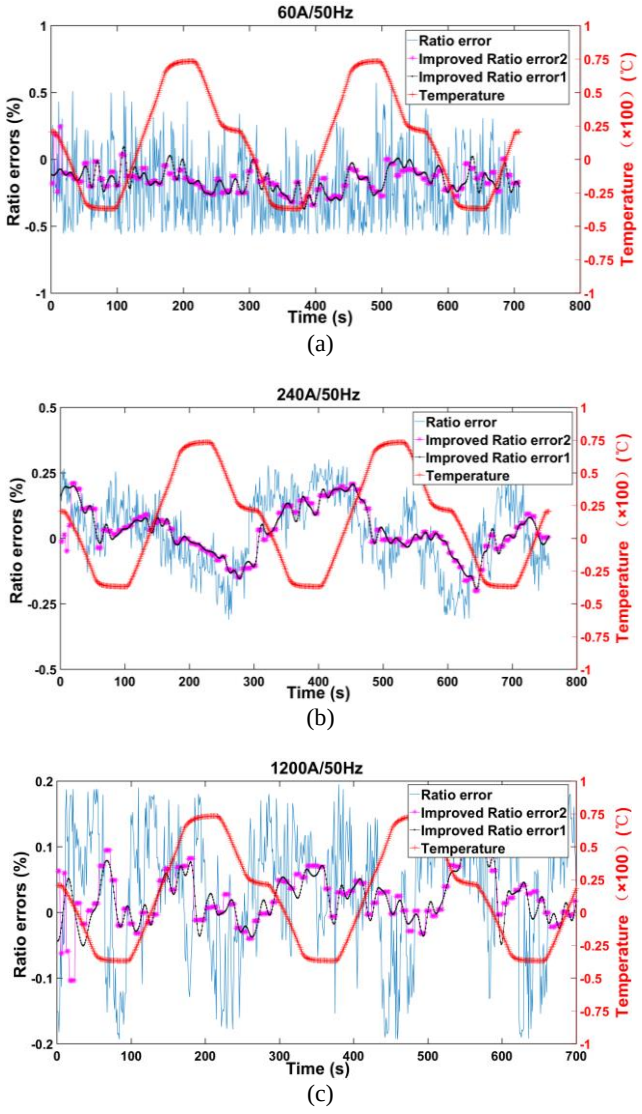

Fig. 4. Ratio errors for different currents: (a) 60A @ 50Hz, (b) 240A @ 50Hz, (c) 1200A @ 50Hz (color online)

In Fig. 4 (b), it can be seen that current size is 240A, fluctuation of ratio error marked by blue symbol '---' curve is within ±0.3%. Fluctuation of ratio error marked by pink symbol '-*-' curve and black symbol '-.-' curve are clearly within ±0.25%. It can be found that three experimental results meet national standards where fluctuation of ratio error is required to be within ±0.35%. However, the result based on CL multi-wavelet combined with variable step-size RLS filter is best, where fluctuation value of ratio error is least and quickly keeps up with current variation in all data. The result based on Haar wavelet combined with conventional RLS filter is better, where fluctuation value of ratio error has left behind the current variation in the starring data. The result based on traditional system is the last, where fluctuation values of ratio error are relatively more 0.05% than those obtained by above two methods.

In Fig. 4 (c), it can be seen that current size is 1200A, fluctuation of ratio error marked by blue symbol '---' curve is within ±0.2%. Fluctuation of ratio error marked by pink symbol '-*-' curve and black symbol '-.-' curve are clearly within ±0.15%. It can be seen that three experimental results meet national standards where fluctuation of ratio error is required to be within ±0.2%. However, the result based on CL multi-wavelet combined with variable step-size RLS filter is best, where fluctuation value of ratio error is least and quickly keeps up with current variation in all data. The result based on Haar wavelet combined with conventional RLS filter is better, where fluctuation values of ratio error have left behind the current variation in the starring data. The result based on traditional system is the last, where fluctuation values of ratio error are relatively more 0.05% than those obtained by above two methods.

It can be found that when temperature quickly changes from -40°C to 75°C for almost ten minutes, the experimental result based on CL multi-wavelet combined with variable step-size RLS filter is best for the FOCTS.

4. Conclusions

In this paper, a new hybrid adaptive filtering full optical current transformer system based on tristate polarization diversity receiver is proposed. We used Jones vector method to calculate the polarization state along the improved FOCTS. Power and phase difference along the new FOCTS are obtained. The experiment occurred between -40°C and 75°C for about 10 minutes and testing results show ratio errors can meet national standards. Specifically, in the 60A@50Hz, ratio errors obtained by CL multi-wavelet combined with variable step-size RLS filter is less nearly 3 times than those obtained by traditional scheme. In the 240A@50Hz, ratio errors obtained by CL multi-wavelet combined with variable step-size RLS filter is less almost 1.4 times than those obtained by traditional scheme. In the 1200A@50Hz, ratio errors obtained by CL multi-wavelet combined with variable step-size RLS filter is less nearly 1.3 times than those obtained by traditional scheme. The new proposed hybrid adaptive filtering FOCTS based on tristate polarization diversity receiver can be best used to the high current sensing system.

Acknowledgments

This research was supported by Provincial Natural Science Foundation of Hubei (No.2017CFB685). Hubei University of Technology Doctor Research Funding (No.00026). Hubei University of Technology "Advanced Manufacturing Technology and Equipment" Collaborative Innovation Center Open Research Fund (No.1201501 and

No.1201803). Hubei University of Technology Green Industry Technology Leading Project (CPYF2017002, No. 00040). Research Project of Hubei Provincial Department of Education (T201405). Research Project of Hubei Provincial Department of Education (D20181401).

References

[1] D. Xu, W. Sae-Kok, A. Vujanic, A. Motta, N. Powers, T. Neo, 2019 IEEE PES GTD Grand International Conference and Exposition Asia (GTD Asia) **1**, 982 (2019).
[2] M. M. Xue, B. Shen, D. L. Chen, Y. Wang, T. H. Shi, H. H. Wang, Y. W. Sun, J. P. Qiana, H. Xiao, B. J. Xiao, Fusion Engineering and Design **140**, 11 (2019).
[3] Xinxing Gao, Bin Zhao, Optics and Lasers in Engineering **123**, 53 (2019).
[4] Doğuş Karabulut, Anton Miazin, Andrei Gusarov, Philippe Moreau, Willem Leysen, Patrice Mégret, Marc Wuilpart, Fusion Engineering and Design **138**, 48 (2019).
[5] Yonggang Li, Ying Song, 2010 5th International Conference on Critical Infrastructure (CRIS) **2**, 1 (2010).
[6] W. Zhao, S. C. Chan, TENCON 2015-2015 IEEE Region 10 Conference **1**, 1-3 (2015).
[7] Aritra Chatterjee, Iti Saha Misra, 2015 IEEE Power, Communication and Information Technology Conference (PCITC) **1**, 1-6 (2015).
[8] Xiang Liu, Xiaozhou Wang, Hao Xiao, Boyang Liu, 20147 China International Conference on Electricity Distribution (CICED) **3**, 1519 (2014).
[9] Xiaxiao Wang, Yuning Zhang, Jia Yu, Yangyang Gao, Optik **127**(7), 8505 (2016).
[10] Xiang Liu, Hao Xiao, Jing Dai, Keqin Guo, Fan Yang, Xiaozhou Wang, Pen Chen, 2014 International Conference on Power System Technology **3**, 1895 (2014).
[11] Yan Xu, Yao Li, Xia Xiao, Zili Xu, Haoliang Hu, Measurement **112**, 117 (2017).
[12] Zhangting Huang, Hao Zhang, Junzhen Jiang, Yishen Qiu, Weijun Li, Optical Fiber Technology **32**, 1 (2016).
[13] Pengyuan Qian, Shuangbao Wang, Yujie Wang, Optical Materials **89**, 349 (2019).
[14] Q. Tao, Lasers in Engineering **32**(1-2), 37 (2015).
[15] Huizu Lin, Lina Ma, Yongming Hu, Wei Wang, Optik **124**(21), 4976 (2013).
[16] Fangmei Gu, Yingchun Li, Yingxiong Song, Jian Chen, Minjie Zhang, Optics Communications **435**, 140 (2019).
[17] Wenhua Zhang, Zhen Guo, Kan Gao, Jianbo Sha, Zhiguo Dai, Shaoling Zhou, 2017 16th International Conference on Optical Communications and Networks (ICOCN) **1**, 1-3 (2017).
[18] V. Rymanov, B. Khani, S. Dülme, A. Stöhr, 2015 European Conference on Optical Communication (ECOC) **1**, 1-3 (2015).
[19] Wentai Lin, Shuqin Lou, Sheng Liang, Optik **125**(3), 942 (2014).
[20] Georges Kesserwani, James Shaw, Mohammad K. Sharifian, Domenico Bau, Jennifer K. Ryan, Advances in Water Resources **129**, 31 (2019).
[21] Rahim Barzegar, Elham Fijani, Asghar Asghari Moghaddam, Evangelos Tziritis, Science of the Total Environment **599–600**, 20 (2017).
[22] Xiao-Guang Gao, Zhi-Gao Guo, Hao Ren, Yu Yang, Chu-Chao He, International Journal of Approximate Reasoning **108**, 62 (2019).
[23] Xudong Yao, Journal of Computational and Applied Mathematics **342**, 495 (2018).
[24] Camelia Elisei-Iliescu, Cristian Stanciu, Constantin Paleologu, Jacob Benesty, Silviu Ciochină, Digital Signal Processing **83**, 280 (2018).
[25] Lin Gan, He Zhang, Optik **171**, 543(2018).
[26] Chinese GB 1208-2006 current transformers national standard (2003), IEC 60044-1:2003, Instrument transformers - Part 1: Current transformers, MOD.
[27] Q. Tao, D-M. Peng, Lasers in Engineering **37**, 95 (2017).

*Corresponding author: dun.liu@hbut.edu.cn